TREATING MACROPHAGES WITH ANTI-INFLAMMATORY NANOPARTICLES AS A STRATEGY TO IMPROVE MUSCLE REPAIR

Presented by Derek Yan

In partial fulfillment of the requirements for graduation with the Health Science Honors Degree in Biochemistry

_____ _____

Laura Suggs
Supervising Professor

Date

_____ _____

Jeffrey E. Barrick

Date

I grant the Health Science Scholars permission to post a copy of my thesis on the Texas Scholarworks. For more information, visit https://repositories.lib.utexas.edu/.

Treating Macrophages with Anti-Inflammatory Nanoparticles as a Strategy to Improve Muscle Repair

Department: Biochemistry/Biomedical Engineering

_____ _____

Derek Yan Date

_____ _____

Laura Suggs, Supervising Professor Date

TABLE OF CONTENTS

Acknowledgements

I would like to thank my graduate student mentor, Chelsea Kraynak, for introducing me to lab techniques and working with me to plan out the direction of my thesis. While working with her, I obtained the skills necessary for performing experiments and learned a great deal about immunology. Her guidance was instrumental for my completion of my thesis.

I would also like to thank Dr. Suggs and the rest of the Suggs Lab for being so welcoming as I joined a lab in a department with which I had few connections in. Dr. Suggs provided guidance that made me keep my research relevant to my goals. The other graduate students in the lab have also never failed to help and encourage me.

Treating Macrophages with Anti-inflammatory Nanoparticles as a Strategy to Improve Muscle Repair

Abstract

The macrophage is an immune cell that is involved in host defense. More recent research, however, has revealed that they also play a central role in mediating the skeletal muscle regenerative process. Upon muscle injury, macrophages are recruited to the damaged site and begin differentiating into a pro-inflammatory phenotype, known as the M1 phenotype. M1 macrophages secrete inflammatory cytokines to facilitate the acute response to muscle injury, and are characterized by phagocytosis of cellular debris and exhibiting strong microbicidal activity. However, another hallmark of inflammatory macrophages is the metabolism of arginine into nitric oxide (NO), which is further metabolized into other reactive oxygen species such as superoxide and peroxynitrite. If left unchecked, prolonged macrophage inflammation leads to muscle cell lysis due to the persistence of reactive oxygen radicals. The capacity of macrophages to stimulate myogenic cells to proliferate is also reduced if inflammation persists. To improve muscle regeneration, we have developed and synthesized a nanoparticle formulation that allows controlled reduction of macrophage inflammatory phenotype. Previous published studies have shown lactic acid and magnesium as chemical agents that attenuate M1 phenotype in macrophages. We developed a poly-lactic-co-glycolic acid (PLGA) nanoparticle emulsified with magnesium sulfate to attenuate the inflammatory phenotype in a murine macrophage cell line. This Magnesium-PLGA nanoparticle has been optimized to be uptaken by macrophages without affecting cell viability. We hope that these contributions make the first steps towards developing an injectable therapy to modulate macrophage phenotype, and can be used in conjunction with existing treatments to improve skeletal muscle repair following injury.

Introduction and Background

Skeletal muscle injury is the most common sports-related injury, accounting for up to 55% of all acute sports injuries [1]. These injuries are sustained through direct trauma (by taking the form of lacerations, strains, and contusions) and through indirect trauma (related to ischemia) [2]. However, the treatment of these injuries remains as a challenge in primary care and sports medicine due to the debate in literature over the optimal treatment. PRICE (protection, rest, ice, compression, and elevation) therapy, stretching, and physical therapy are among the commonly used treatments for skeletal muscle injury [3]. We aim to develop an injectable therapy that can be used in conjunction with existing treatments to further improve the muscle repair process. By targeting macrophage-mediated inflammation in the context of muscle repair, tissue regeneration is improved.

Stages of Skeletal Muscle Repair

Skeletal muscle repair following injury has been classically categorized into three stages- the degenerative/inflammatory phase, the regenerative/anti-inflammatory phase, and the remodeling phase [4]. The inflammatory phase occurs within the first few days after muscle tissue homeostasis is disrupted. Immediately following skeletal muscle injury, myofibers necrotize and surrounding blood vessels rupture, forming a hematoma. As a result of muscle cell death, cytokine release occurs and blood-borne immune cells extravasate into the site of injury through the hematoma. Neutrophils are the first inflammatory cells to infiltrate, and they secrete cytokines TNF-α and IL-6 and

growth factors to create a chemoattractive environment for monocytes and macrophages [5]. Once macrophages arrive at the site of injury, these cytokines and other extracellular cues drive their inflammatory response. Infilitrating macrophages and monocytes become primarily responsible for directing inflammation and the transition to the second stage.

The second stage, the regenerative phase, typically begins 3-5 days after injury. Muscle regeneration peaks at 2 weeks following injury, and slowly diminishes as it approaches 3-4 weeks post-injury [6]. Because muscle fibers are comprised of cells that are post-mitotic, injured fibers require adult muscle stem cells (MSCs) to be repaired. Through a complex set of regulatory mechanisms, MSCs activate and proliferate to generate a robust population of myoblasts that differentiate to repair injured myofibers and self-renew to maintain the myoblast count [7].

The final remodeling phase completes repair following injury; connective scar tissue eventually forms, along with vessel and neural growth. Growth factors are heavily involved in facilitating this process, as transforming growth factor β1 causes significant fibroblast proliferation and vascular endothelial growth factor promotes angiogenesis [8].

Significance of Macrophages in Muscle Repair

Macrophages perhaps are the most important immune cell in regulating muscle repair, especially throughout the first two stages. Several roles have been identified as: phagocytosing cellular debris, directing the shift from the degenerative to regenerative phase through paracrine signaling, preventing muscle cell apoptosis, releasing factors to promote myogenic precursor cell proliferation, and secreting cytokines to facilitate

vascular and myofiber repair [9]. They have been well studied and have been shown to be absolutely necessary for adequate skeletal muscle regeneration. Multiple studies either depleted macrophage precursor cells or attenuated their migration and show that muscle regeneration following injury is dramatically impaired [10, 11, 12]. As a key player to the muscle healing process, macrophages are an extremely promising candidate to study to improve muscle repair.

Traditionally, matured macrophages have been classified into its two distinctive phenotypes, the classically activated macrophage (M1) and the alternatively activated macrophage (M2) [13]. A resting macrophage that has not matured is typically known as M0. The M1 phenotype is characterized by high expression of pro-inflammatory cytokines such as TNF-α and IL-1β, production of reactive nitrogen and oxygen intermediates through the arginase pathway, and strong microbicidal activity [14]. Also known as inflammatory macrophages, M1 macrophages dominate at the site of injury for a few days following skeletal muscle trauma. In contrast, M2, or anti-inflammatory macrophages, primarily act 2-4 days following injury. They attenuate the inflammatory response by readily expressing scavenging molecules, producing ornithine and polyamines through the arginase pathway, and containing parasites [14]. Following the reduction of inflammation, M2 macrophages initiate muscle repair by encouraging MSC proliferation and stimulating their commitment to into myocytes [15]. Perhaps the greatest evidence that these phenotypes compete with each other to regulate inflammation is the well-studied macrophage metabolism of arginine, which can diverge into two pathways. M1 macrophages metabolize arginine via inducible nitric oxide synthase (iNOS) into nitric oxide (NO) and citrulline, whereas M2 macrophages

metabolize arginine via arginase into ornithine and urea [16]. This competition for limited arginine is a hallmark of the M1/M2 macrophage dichotomy.

Despite the divisive features that identify the M1 and M2 phenotype, plasticity and flexibility also define macrophages. A macrophage that expresses M1 phenotype does not necessarily maintain that fate; extracellular cues can shift macrophage phenotype regardless of maturation status. Moreover, macrophage phenotype is typically not absolute M1 or M2. The phenotype is able exist in a state that falls within both categories of macrophages. The process of a macrophage transitioning into a different phenotype is known as polarization. Interestingly, polarized M1 and M2 macrophages can have their phenotypes almost completely reversed in vitro and in vivo [17, 18]. At the site of muscle injury, the macrophage population consists of coexisting M1 and M2 phenotypes, with a higher proportion of M1 macrophages during the first two days after injury but a higher proportion of M2 macrophages 2-4 days post-injury as polarization occurs. The activation and release of M2 associated genes and cytokines such as IL-10 and TGF-β further cause a shift away from inflammation to produce an environment conducive of muscle repair. However, previous experiments have shown that inducing earlier shift to M2 dominance during the muscle repair process significantly improved tissue recovery, while delaying M2 polarization impaired tissue regeneration [19, 20]. This evidence is supported by the high metabolism of arginine into reactive nitric oxide by M1 macrophages. Nitric oxide is metabolized into other reactive oxygen species such as superoxide and peroxynitrite; their prolonged circulation in the site of muscle injury contributes to muscle cell lysis [21]. We took interest in these findings and investigated strategies to induce a more robust transition

towards an M2-polarized macrophage population within the first few days of skeletal muscle injury as our strategy to improve muscle repair. This began the search for a readily available, biocompatible chemical agent capable of targeting macrophages to promote M2 polarization.

Selection of Chemical Factors

It is widely accepted that tumor-associated macrophages (TAMs) adopt a M2-like phenotype, but specific intra-tumoral signaling that drives these phenotype remains unclear. In a recent experiment, researchers used a murine model to identify lactic acid as a signaling molecule that induces the expression of multiple M2-associated genes in TAMs [22]. This finding was mirrored in another study that showed the induction of human-derived macrophages to M2 phenotype by tumor-derived lactic acid in vitro [23]. We chose lactic acid as the readily available factor that promotes M2 phenotype.

In addition to stimulating macrophages towards M2 phenotype, an accelerated reduction of M1 phenotype should help resolve inflammation. Recent research shows strong evidence that magnesium salts are capable of diminishing the activation of nuclear factor-κB (NF-κB), an inducible transcription factor responsible for regulating the transcription of a large number of key inflammatory genes [24]. NF-κB activation leads to production of inflammatory cytokines and adhesion molecules and the regulation of cell proliferation, apoptosis, and morphogenesis [25]. Its pro-inflammatory function is widely recognized and has been well studied in macrophages [26]. By delivering appropriate concentrations of lactic acid and magnesium to macrophages, we expected to be able to reduce inflammation while promoting M2 polarization. However,

the challenge remains to develop a method of targeting macrophages to deliver these soluble factors with minimal off-target effects. A biocompatible drug carrier is required for this purpose.

Nanoparticle Design

We chose to design a nano-sized particle that is stable in biological solutions. Nanoparticles are currently being used in medicine to improve the target efficiency of drugs because their size, shape, and surface properties are flexible and can be engineered in different ways [27.28]. Although the nanoparticle surface can be modified with antibodies or peptides to grant extremely specific targeting, we relied on optimizing the particle size and shape to target macrophages and avoid any undesired side immune responses. Macrophages are the primary scavengers of foreign material in the body, and have a higher capacity for engulfing foreign debris than other cell types. We exploited this characteristic of macrophages by developing spherical nanoparticles of appropriate size.

We used poly-lactic-co-glycolic acid (PLGA) as the polymer to develop a biocompatible nanoparticle suitable for our goals. PLGA, which is biologically stable yet biodegradable, has been used during the last two decades as one of the most attractive polymeric candidates for controlled drug delivery [29]. It hydrolyzes into its two components, lactic acid and glycolic acid, on the order of several days. The rate of hydrolysis increases as the pH of its environment becomes more acidic [30]. Moreover, PLGA can be controlled to exist in different ratios of lactic acid to glycolic acid; as this ratio increases, the rate of hydrolysis decreases [31]. We used PLGA at a ratio of 50% lactic acid to 50% glycolic acid for our nanoparticle design.

The stability of PLGA in biological solutions makes it an appropriate drug carrier for our therapy. In general, spherical nanoparticles are formed from PLGA by dissolving PLGA in an organic solvent and emulsifying it in an aqueous phase, typically water. PLGA droplets disperse throughout the emulsion, and the emulsion is given time to allow the organic solvent to evaporate out of solution. This process causes the PLGA droplets to precipitate and harden into smaller spheres, which forms PLGA particles. The size of these particles is dependent on the initial PLGA concentration in the organic phase and the organic solvent being used [32]. We denote PLGA that has been synthesized without incorporating a stabilizer or other chemical agent as bare PLGA.

To incorporate magnesium into our PLGA nanoparticle, we used a water-in-oil-in-water (w/o/w) double emulsion to entrap magnesium sulfate in the PLGA [33]. Particle size was optimized so that the macrophages would uptake them through endocytosis, because phagocytosis has been shown to be coupled with inflammation [34]. As the macrophages take up and concentrate Mg-PLGA in their endosomes, the environment acidifies, leading to a higher rate of hydrolysis and a higher concentration of intracellular lactic acid. Entrapped magnesium is also released in the cell, allowing both soluble factors to stimulate the cell. We hypothesize that our Mg-PLGA nanoparticles can effectively target macrophages to reduce inflammatory phenotype while promoting M2 polarization. This strategy lowers the necessary dose of magnesium sulfate and lactic acid than if these factors were to be injected in their soluble form. Moreover, off-target effects are avoided through the incorporation of a nanoparticle that is stable in biological solutions.

Glossary

Inflammatory Cytokines and Genes

IL-6: Interleukin-6. A cytokine that is the chief stimulator of acute phase proteins, which respond to inflammation. A change in acute phase protein levels indicates the presence and intensity of inflammation [36]. However, IL-6 has been implicated to reinforce, although not trigger, M2 polarization in macrophages that were already being induced towards alternative activation [37].

IL-1β: Interleukin- 1β. This cytokine plays a key role in the induction of early immune response to inflammatory stimuli, including tissue injury. IL-1β has been shown to have the ability to activate the NF-κB promoter [38].

iNOS gene: inducible Nitric Oxide Synthase. iNOS is highly expressed in inflammatory macrophages. The enzyme is responsible for the production of nitric oxide by catalyzing the metabolism of arginine. LPS and IFN-γ heavily induce iNOS expression [39].

TNF-α: Tumor necrosis factor-α. A cytokine that is a “master regulator” of inflammatory cytokine production and orchestrates inflammatory cascades. Macrophages are the primary producers of TNF-α and are highly responsive to TNF-α [35].

Anti-inflammatory Cytokines and Genes

Arg1 gene: Arginase isoform 1. Arg1 competes with iNOS for arginine; Arg1 metabolizes arginine into ornithine and and urea. Arg1 is classically known as a M2 macrophage marker [40].

IL-10: Interleukin-10. An important anti-inflammatory cytokine that inhibits expression of TNF-α and IL-6 in macrophages [41]. IL-10 has been demonstrated to reduce inflammation in animal models of sepsis [42].

Macrophage Activation

IFN-γ: Interferon-γ. Major M1 stimuli that has been widely used for macrophage polarization. IFN-γ activates macrophages through the signal transducer and activator of transcription 1 (STAT1) signaling pathway [43].

LPS: Lipopolysaccharide. An M1 stimulus that activates macrophages through the toll-like receptor (TLR) signaling pathway [43]. Found on the surface of gram-negative bacteria.

Methods

Murine model cell line

RAW 264.7 macrophages, an Abelson leukemia virus transformed cell line, were used throughout the experiments as a model of murine macrophages. Cells were cultured in high glucose DMEM supplemented with 10% heat-inactivated FBS, 1% penicillin/streptomycin, and 1% sodium pyruvate, and incubated at 37°C with 5% CO_2. To maintain the cell line, cells were passaged after reaching 80% confluence, detached with cell scraper and 1-2 million cells were re-cultivated in T-75 flasks. Cells were typically cultured in this fashion until passage no. 25.

3T3 murine fibroblasts were cultured as to model a connective tissue cell line in flow cytometry experiments. To maintain cell line, cells were cultured in high glucose DMEM supplemented with 10% FBS, 1% pencillin/streptomycin, and 1% sodium pyruvate, and incubated at 37°C with 5% CO_2. Cells were passaged after reaching about 80% confluence, detached with trypsin, and re-cultivated in a 1:10 ratio in T-75 flasks.

Macrophage stimulation

In all experiments, macrophages were stimulated either with 100 ng/mL LPS or 20 ng/mL IFN-γ to generate an inflammatory M1 phenotype. M1 stimulants were introduced to macrophages at the same time as any other chemical factor being studied (lactate, $MgSO_4$, Mg-PLGA).

Real time PCR

300,000 cells/well were cultured onto a 6-well plate (9.5 cm^2 growth area) and allowed to adhere overnight. Cells were then stimulated with treatment for 24h. RNA was isolated

using the Qiagen© RNeasy Mini Kit (Cat. No. 74104), and the High-Capacity RNA-to-cDNA™ Kit (Cat. No. 4387406) from Applied Biosystems™ was used for reverse transcription. Quantitative RT-PCR was performed using SYBR™ Green Master Mix from Applied Biosystems (Cat. No. 4309155) and qPCR system. Data was analyzed using the comparative CT method [44]. HPRT was used as an appropriate housekeeping gene.

Griess and MTS assay

30,000 cells/well were cultured onto a 48-well plate (0.95 cm^2 growth area) and allowed to adhere overnight. Cells were then stimulated with treatment for 24h. Supernatant was collected, and samples were centrifuged at 20,000 g to remove excess nanoparticles. Griess reagents were used to indirectly determine the concentration of NO [45]. Through this two-step diazotization reaction, colorimetric determination of NO concentration is carried out by measuring the absorbance at 540 nm on microplate photometer. Raw absorbance values were converted to NO concentrations through a standard. To account for differences in cell viability between groups, MTS assay was performed on the cells after supernatant was removed [46]. MTS reagent, tetrazolium, is enzymatically reduced in metabolically active cells to generate a colored formazan product. The product absorbs light strongly at 490 nm, and the absorbance intensity is measured to quantify relative metabolic activity. 2 hours of incubation was allowed for MTS treatment to ensure that the reagent had not been completely metabolized. Absorbance values obtained from MTS were used to normalize NO concentration to cell viability.

Nanoparticle synthesis

Magnesium was entrapped into PLGA nanoparticles using a double emulsion protocol [33]. Dichloromethane (DCM) was used as the organic solvent. 50 μL of saturated $MgSO_4$

solution at room temperature was added into 50 mg of dissolved PLGA in DCM to form the initial emulsion. Poly-vinyl alcohol (PVA) was used as the stabilizing agent. Because the concentration of stabilizing agent used in the vortexing emulsification step primarily controls the size of the nanoparticles that form, 5% PVA was used in this step to create nanoparticles of appropriate size [33]. Nanoparticles were decanted into a stirring solution of 45 mLs of 0.3% PVA and left for 3 hours for DCM to evaporate and nanoparticles to harden. Nanoparticles were centrifuged at 20,000 g and resuspended in water to remove soluble magnesium and residual PVA.

Fluorescent nanoparticle synthesis

Fluorescent PLGA nanoparticles were synthesized for flow cytometry and confocal images. DiI, an indocarbocyanine dye, was incorporated into PLGA nanoparticles for flow cytometry while DiO, an oxacarbocyanine dye, was incorporated into PLGA nanoparticles for the confocal images. For synthesis of fluorescent nanoparticles, the dye was dissolved with PLGA and 1% w/v F-127 Pluronic into the organic phase, and then emulsified with 5% PVA. Fluorescent PLGA nanoparticle synthesis matched magnesium PLGA nanoparticle synthesis otherwise to serve as a detectable representation.

Flow cytometry

RAW and 3T3 cells were co-cultured into 6-well plates at 300,000 total cells/well, and 150,000 cells of each respective cell type. High glucose DMEM supplemented with 10% heat-inactivated FBS, 1% penicillin/streptomycin, and 1% sodium pyruvate was used as appropriate media for both cell types. Cells were allowed to adhere overnight, and treatment was given the following day either for 3h or 24h. Following treatment, were stained with APC-Cy7 anti-mouse F4/80 antibody, which is a commonly used antibody as

a macrophage marker. Cells in the 3h treatment groups were fixed with 2% paraformaldehyde so that flow cytometry could be performed on both the 3h and 24h timepoints concurrently.

TEM

Nanoparticles were immobilized on plasma-treated carbon grid, and residual solution was removed with blotting paper. They were then negative-stained with uranyl acetate to improve contrast, and were imaged on a FEI Tecnai Transmission Electron Microscope.

Dynamic Light Scattering (DLS) and Zeta

A Zetasizer instrument was used to perform DLS and Zeta measurements on nanoparticles. Nanoparticles were first washed to remove any excess PVA, which could interfere with light scattering. Following resuspension, nanoparticles were diluted 1:40 in water in disposable cuvettes for DLS. For Zeta, the same diluted particles were placed in capillary cells for measurement.

Confocal images

To prepare for images, fluorescent PLGA nanoparticles were synthesized with DiO, a dye in the same family of dyes as DiI. After treating cells with nanoparticles for 5h, cells were rinsed with PBS and fixed with 2% paraformaldehyde. After thoroughly rinsing off paraformaldehyde, 1 μg/mL DAPI in PBS was added to cells for 5 minutes to allow the dye to bind to DNA for nuclear visualization. After a final rinse with PBS, samples were stored in 4°C overnight and imaged the next day. For imaging, samples were mounted onto a glass cover slip.

Results and Discussion

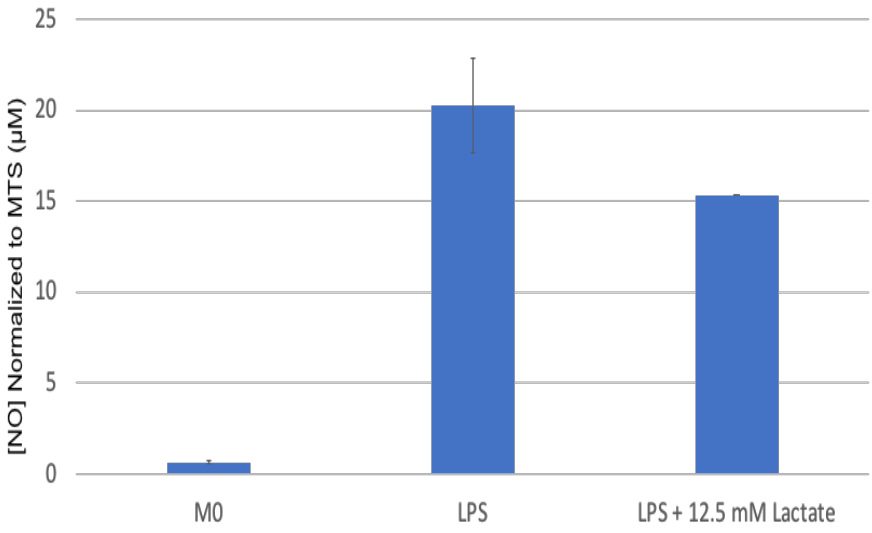

Figure 1. Lactate slightly reduces nitric oxide output in RAW macrophages, indicative of a reduction in NOS activity. Cells were treated for 24h. Following treatment, MTS reagent was introduced to cells and allowed to be metabolized for 2h.

To assess the potency of lactic acid to polarize macrophages towards M2 phenotype, we performed Griess assay on duplicate groups of RAW macrophages and normalized to MTS values as an indirect measure of NOS activity. 12.5 mM lactate was selected as an appropriate, non-toxic concentration after testing multiple concentrations. Macrophages stimulated with LPS only were representative of M1 macrophages. **Figure 1** shows 25% reduction of [NO] output of M1 macrophages stimulated with lactate as compared to M1 macrophages. Data may also suggest that lactate is not extremely effective as a regulator of the TLR-mediated signaling pathway of classical activation, which is stimulated by the presence of LPS in macrophages [43]. Moreover, lactate may have more potency to regulate NOS transcription, rather than translation **(Figure 2)**.

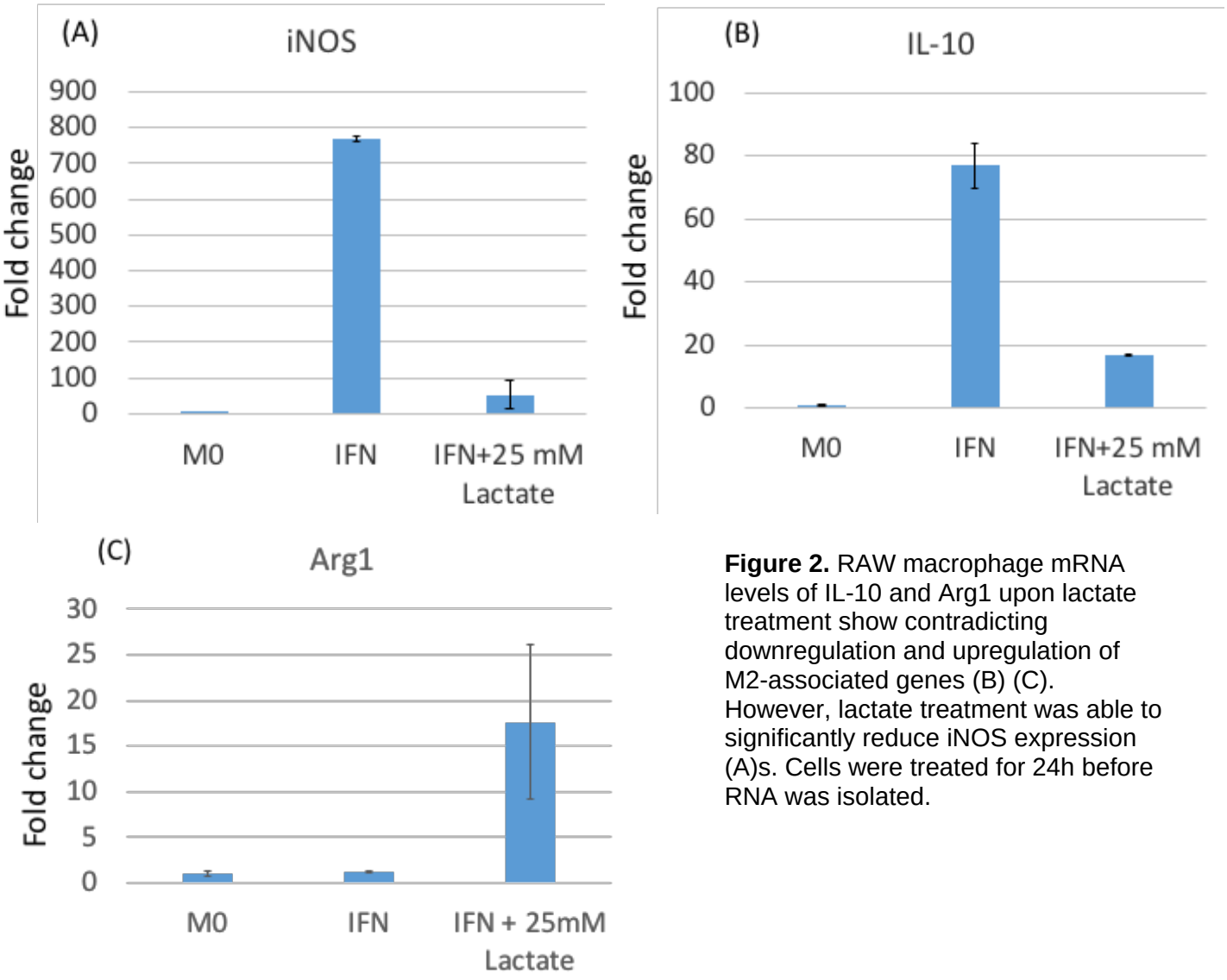

Figure 2. RAW macrophage mRNA levels of IL-10 and Arg1 upon lactate treatment show contradicting downregulation and upregulation of M2-associated genes (B) (C). However, lactate treatment was able to significantly reduce iNOS expression (A)s. Cells were treated for 24h before RNA was isolated.

The effects of lactate on influencing the expression of key M1 genes was investigated by performing RT-PCR on duplicate groups of RAW macrophages stimulated with or without IFN-γ. Cells were stimulated with IFN-γ to identify whether or not a different signaling pathway from TLR is more regulated by lactate. 10-fold reduction of iNOS expression upon addition of lactate suggests that lactate plays a more significant role in regulating the STAT1 pathway to inhibit the expression of a primary M1-associated gene. However, the promotion of M2 phenotype was not as prominent. While Arg1 upregulation

is significant and is consistent with the downregulation of iNOS expression, an approximate 4-fold reduction of IL-10 expression contradicts the promotion of M2 phenotype **(Figure 2)**. This data completes our analysis of soluble lactate as a chemical factor. Lactate is highly promising in reducing NOS levels in macrophages, but we were not able to replicate results that show a conclusive M2-promoting effect.

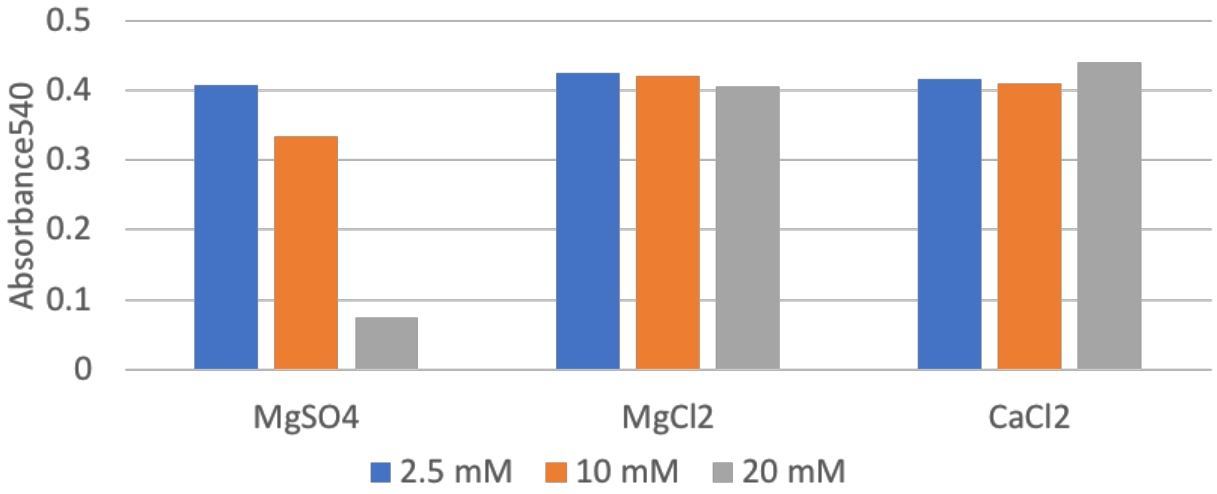

Figure 3. $MgSO_4$ decreases absorbance intensity of Griess reaction in RAWs, while other salts are not capable of doing so. Cells were treated for 24h.

Preliminary testing of different Mg salts on nitric oxide output was performed. RAW macrophages treated with either $MgSO_4$ or $MgCl_2$ upon LPS stimulation showed to respond more to $MgSO_4$ treatment, as shown by Griess assay in **Figure 3**. Both magnesium salts are highly soluble. Only absorbance values of samples were recorded to compare relative absorbance intensities between groups, rather than using standard to obtain nitric oxide concentrations. $CaCl_2$ was an appropriate control to ensure that the divalent salt itself did not change nitric oxide output. Different concentrations were tested to determine dosage, and all three concentrations showed little to no cell toxicity.

$MgSO_4$ had much higher potency to reduce nitric oxide output than $MgCl_2$ did, showing that $MgSO_4$ should be used as the salt to deliver magnesium to macrophages.

M1 macrophages were treated with $MgSO_4$ to reassess the extent to which magnesium can reduce nitric oxide output. Griess assay was performed on duplicate groups. **(Figure 4)** shows significant reduction of [NO] upon addition of $MgSO_4$, with more reduction as the Mg concentration increases. MgSO4 potently reduced nitric oxide, as nitric oxide output of M1 macrophages treated with $MgSO_4$ matched that of macrophages that did not receive LPS treatment.

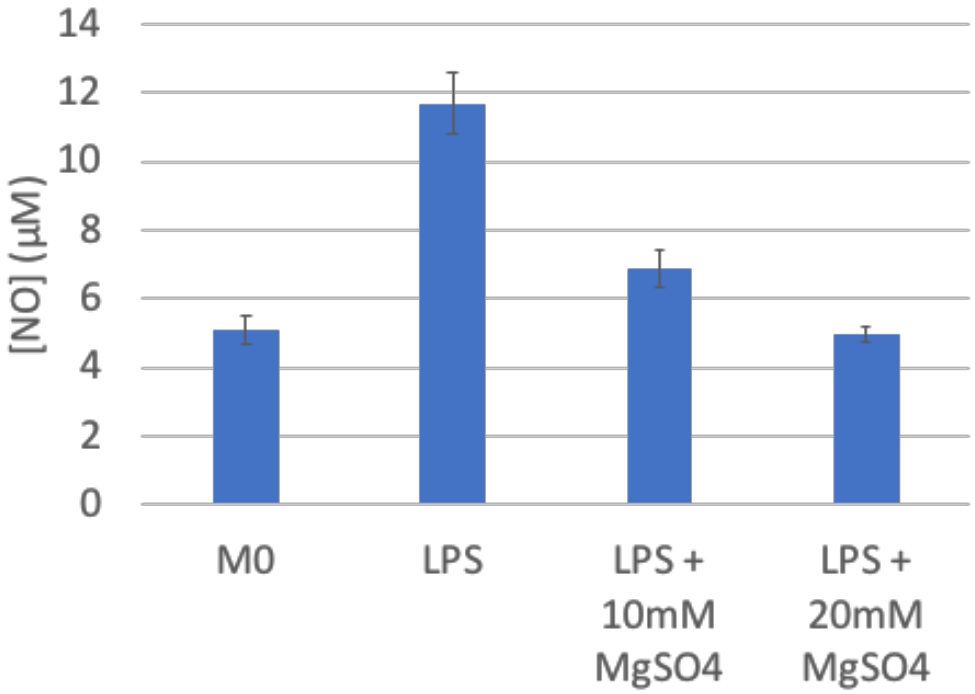

Figure 4. Significant reduction of NOS activity in RAW macrophages upon $MgSO_4$ treatment for 24h. At the 20 mM concentration, nitric oxide output matched that of non-activated macrophages.

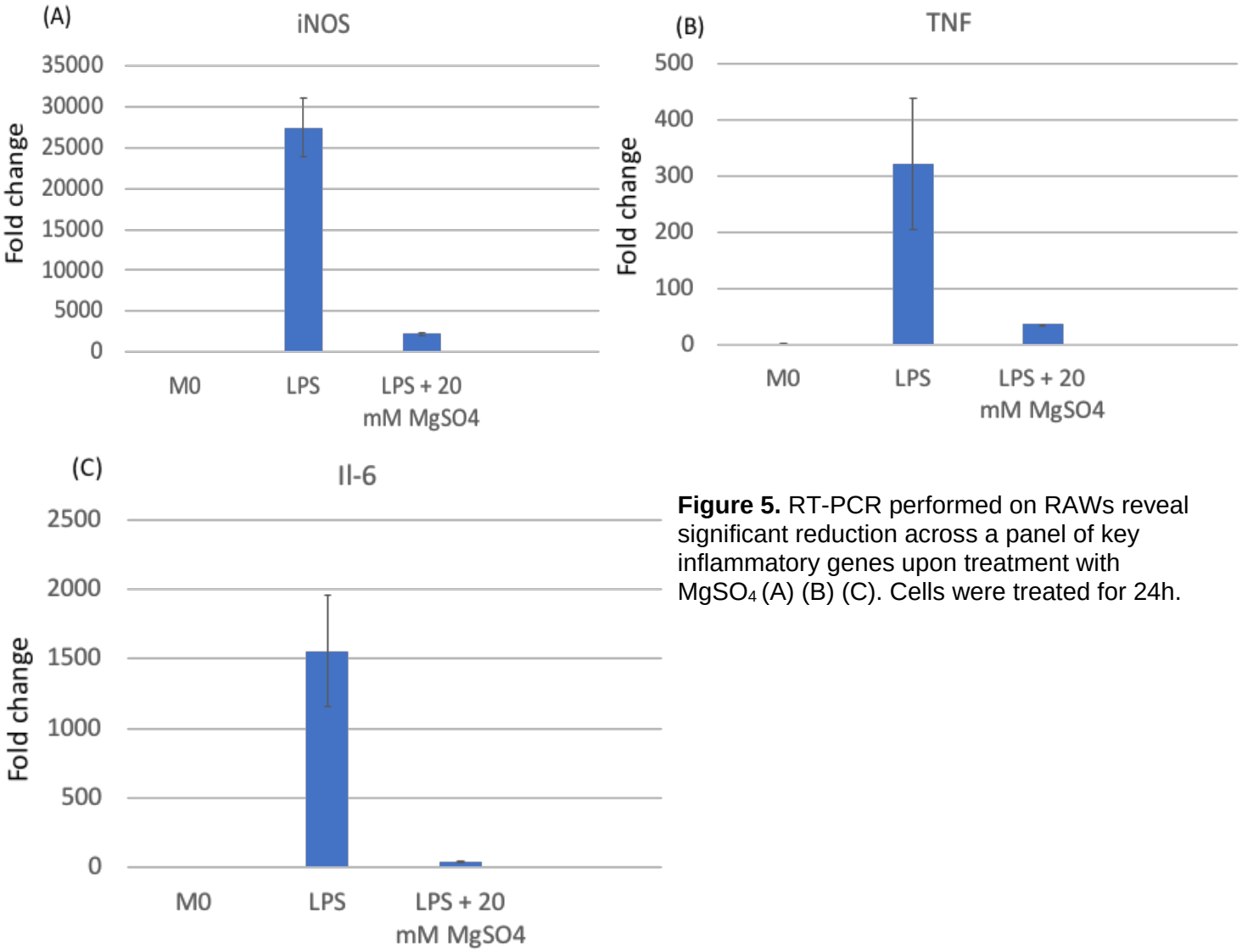

Figure 5. RT-PCR performed on RAWs reveal significant reduction across a panel of key inflammatory genes upon treatment with $MgSO_4$ (A) (B) (C). Cells were treated for 24h.

A set of inflammatory genes was selected to determine the efficacy of $MgSO_4$ in reducing M1 phenotype in RAWs. RT-PCR was performed on duplicate groups of cells. **Figure 5** shows comprehensive reduction of M1 gene expression upon addition of $MgSO_4$. The similar levels of iNOS expression in M0 macrophages and M1 macrophages treated with $MgSO_4$ match the similar levels of NO output shown previously in the Griess Assay. To be able to collectively reduce iNOS, TNF-α, and IL-6 expression without being cytotoxic makes $MgSO_4$ a highly promising agent for

attenuating inflammation. The motivating data shown from the experiments involving magnesium suggest that LPS is an appropriate M1 stimulant to use for following experiments. We then began formation of nanoparticles to co-deliver lactate and magnesium to macrophages.

PLGA nanoparticles are often formed by introducing PLGA dissolved in organic solvent into a larger volume of aqueous solution, forming PLGA droplets. As organic solvent evaporates, the PLGA nanoparticles precipitate into a hardened particle. Without adding any other chemical agents or stabilizers, this process of precipitation creates bare PLGA nanoparticles. The organic solvent being used can be adjusted to control particle size. For our bare PLGA nanoparticle formation, we used acetone as the organic phase and water as the aqueous phase. The nanoparticles generated were about 130-170 nm in diameter, as measured through detection of Brownian motion by the Zetasizer instrument. This size is comfortably smaller than the micron scale, which is typically associated with macrophage phagocytosis [47].

To incorporate magnesium into PLGA nanoparticles, a w/o/w double emulsion method was used. Saturated $MgSO_4$ solution was emulsified into dissolved PLGA in dichloromethane, which was then emulsified with either 0.3% or 5% PVA. Resulting nanoparticles were characterized with Zeta, DLS, and TEM. **Figure 6A** shows that nanoparticles synthesized via the double emulsion protocol consistently had zeta potentials less negative than that of bare PLGA, suggesting that PVA is coating the surface of the nanoparticles and reducing the availability of negatively charged groups in PLGA to interact with surrounding solution. This observation was indicative that PVA is likely not entrapped in the PLGA, which is instead permeated with magnesium.

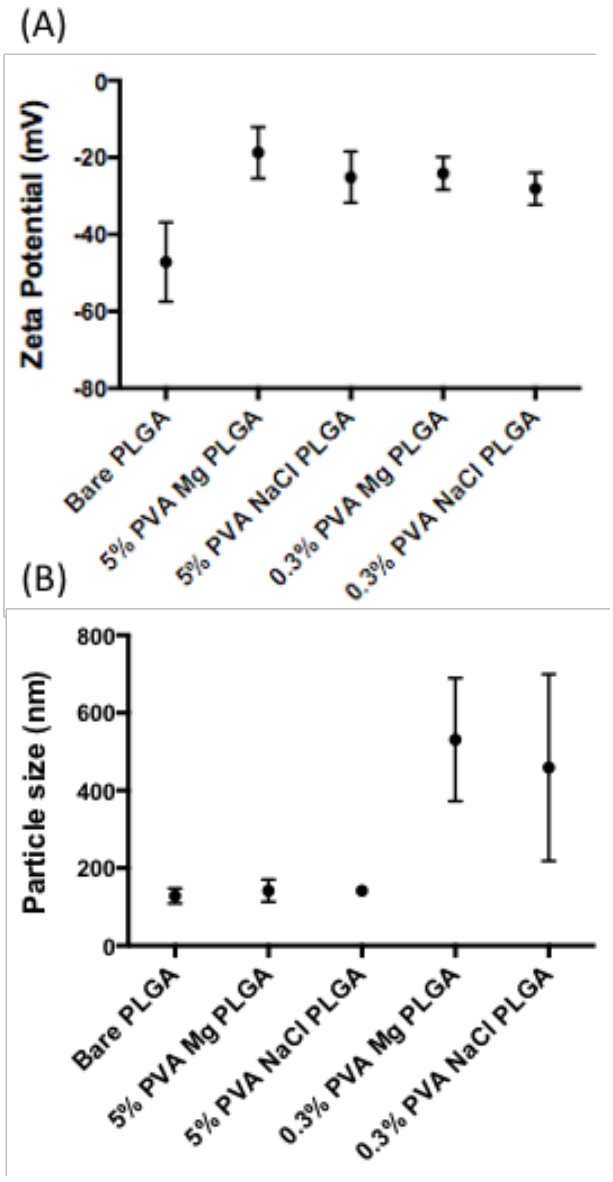

Figure 6. Zeta potential of double emulsion particles show coating of nanoparticle surface by PVA (A). Double emulsion particles synthesized with 5% PVA match the size of bare PLGA, while 0.3% PVA double emulsion particles are much larger and more polydispersed.

The concentration of PVA used to create the second emulsion heavily influences the resulting size of nanoparticles; as this concentration increases, nanoparticle size decreases. The viscosity of the PVA solution determines the shear force applied to the nanoparticles during vortexing. It was reported that PLGA dissolved in dichloromethane emulsified into 5% PVA generated 140 nm diameter nanoparticles [33]. We confirmed this finding by using DLS to measure hydrodynamic diameter of our double emulsion particles synthesized with 5% PVA. **Figure 6B** shows that these nanoparticles had a diameter of approximately 150 ± 20 nm. NaCl PLGA double emulsion particles were synthesized with the same double emulsion protocol. We dissolved NaCl in water at a concentration that matched the concentration of the saturated $MgSO_4$, and dissolved PLGA.

The size of these 5% PVA nanoparticles was nearly identical to the size of the bare PLGA, suggesting that any coating of the surface of the nanoparticles by PVA is

not extremely significant. This thin coating was appropriate, as the small particle size was maintained to avoid triggering phagocytic cell mechanisms. In contrast, the nanoparticles synthesized with only 0.3% PVA began approaching micron size, and had rather high polydispersity. **Figure 7 and 8** confirm the size differences between 5% and 0.3% PVA synthesized nanoparticles.

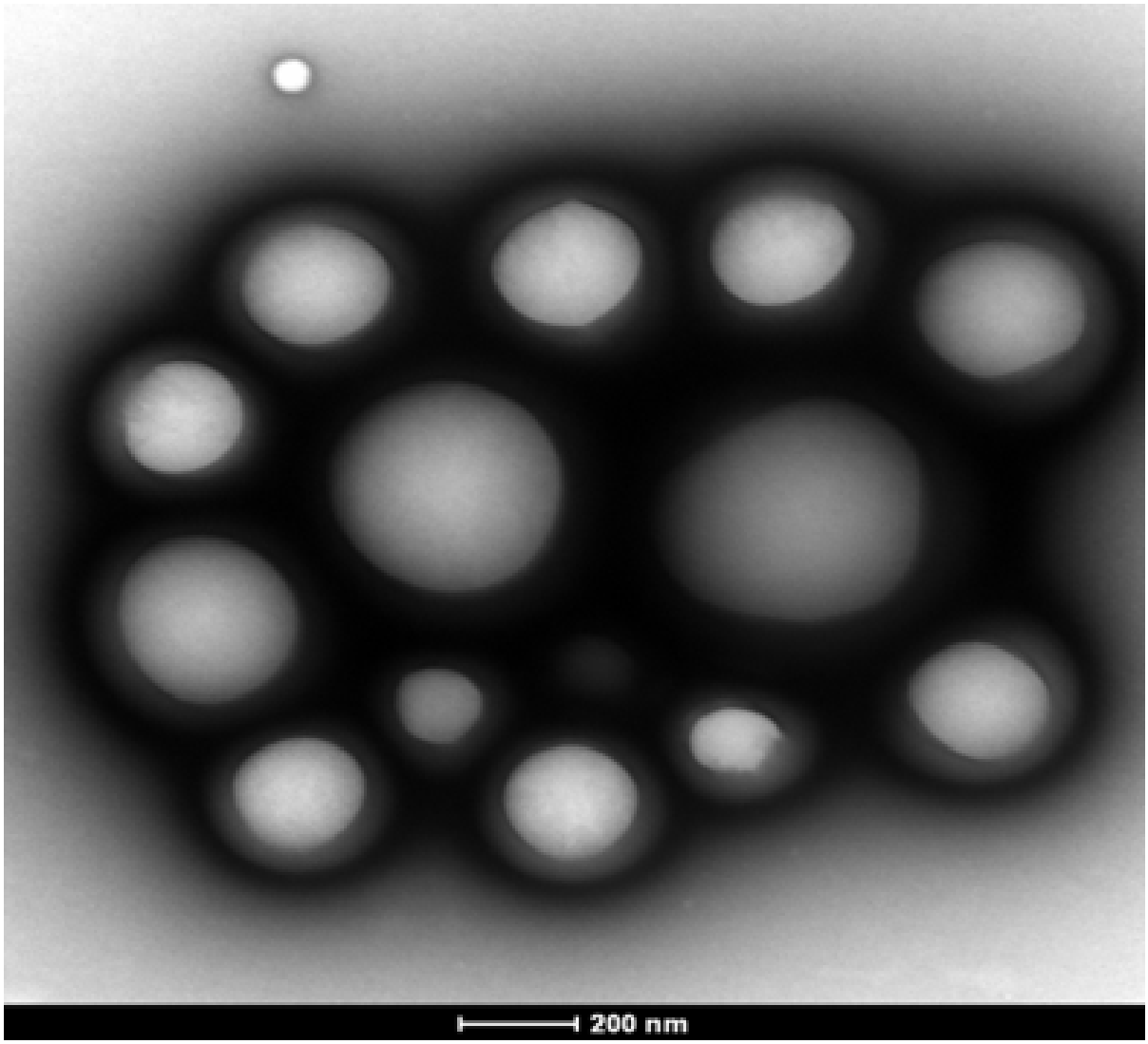

Figure 7. TEM image of Mg PLGA double emulsion nanoparticles synthesized with 0.3% PVA during vortexing step. Scale bar = 200 nm.

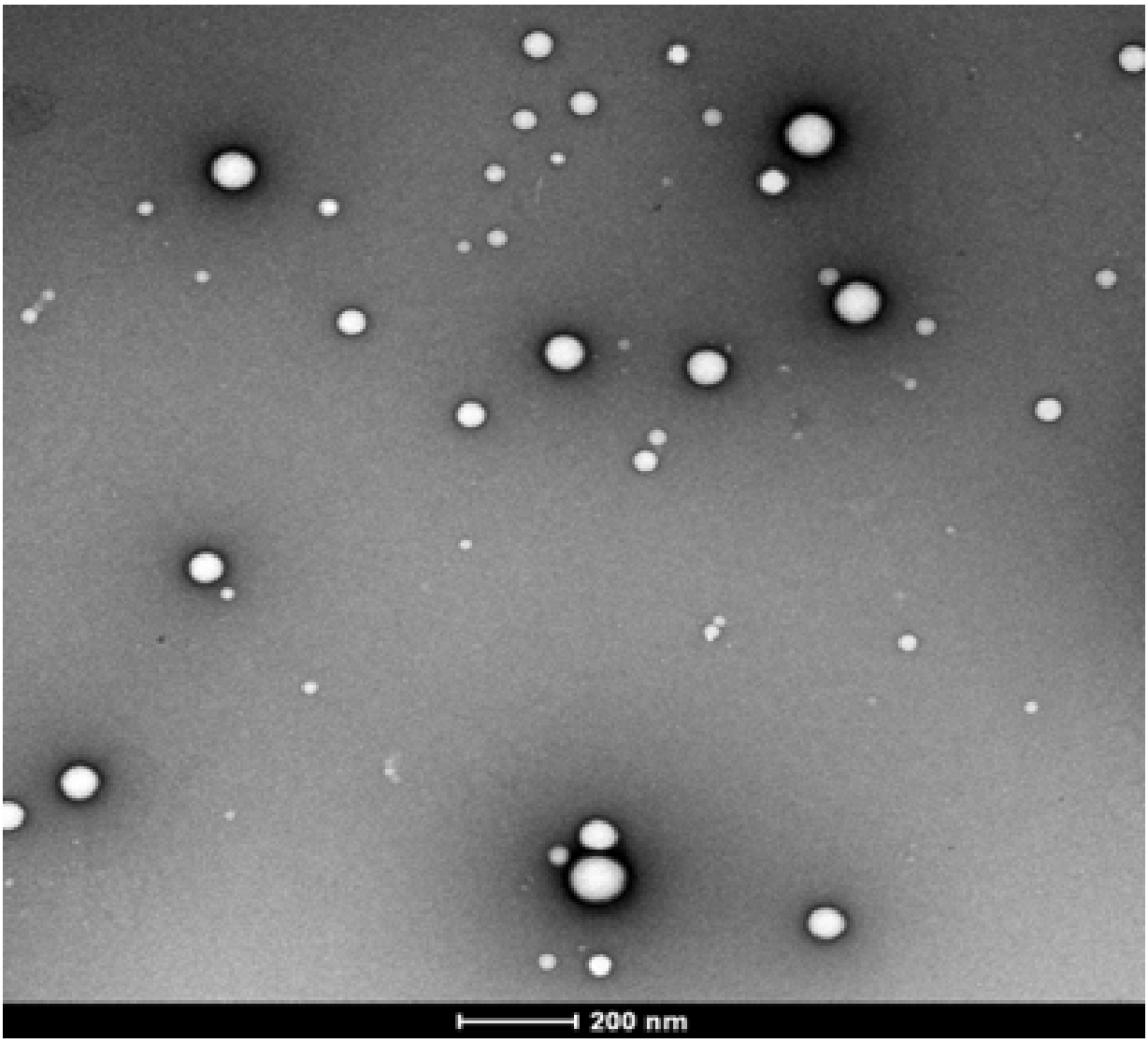

Figure 8. TEM image of Mg-PLGA nanoparticles synthesized with 5% PVA during vortexing step. Scale bar = 200 nm.

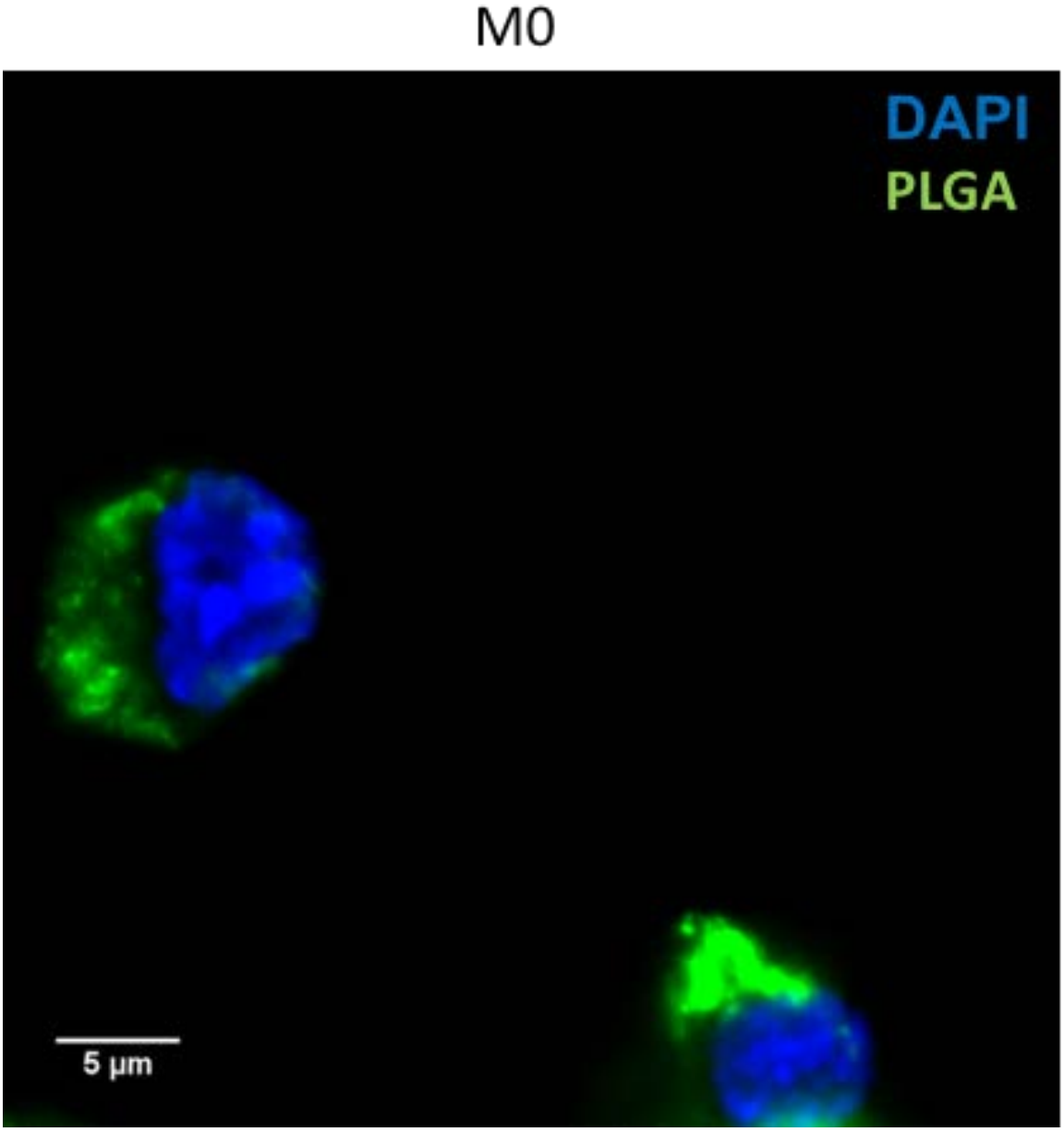

Figure 9. Confocal image of non-activated RAWs treated with DiO PLGA nanoparticles for 5h. Cell nuclei were stained with DAPI. Nanoparticles are shown concentrated outside cell nuclei. Image analyzed with ImageJ.

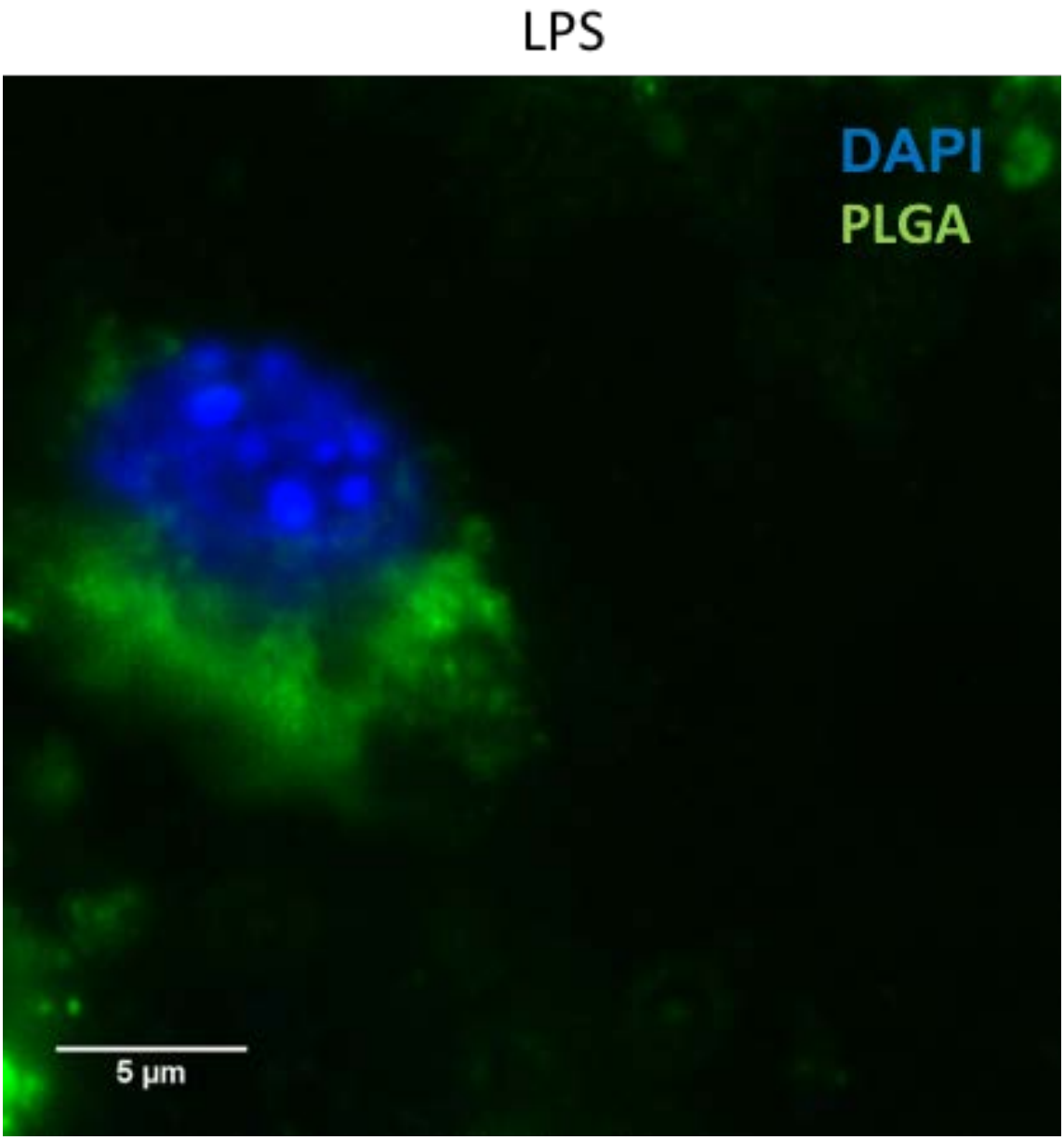

Figure 10. Confocal image of activated RAWs treated with DiO PLGA nanoparticles for 5h. Cell nuclei were stained with DAPI. Nanoparticles are shown concentrated outside cell nuclei. Image analyzed with ImageJ.

DiI fluorescent nanoparticles were synthesized for analysis in flow cytometry. 0.05% w/v DiI was added to dissolved PLGA and F-127 Pluronic in DCM, and then emulsified with 5% PVA to generate nanoparticles that mimic previously generated Mg PLGA nanoparticles. To assess the stability of DiI fluorescent PLGA nanoparticles, a fluorescence-over-time experiment was performed. After nanoparticles were washed, they were resuspended in 1% BSA in PBS, representative of cell media. Duplicates of three groups were tested. The 0h group was immediately centrifuged to pellet. Tubes were placed in 4°C for storage. The 4h and 24h groups were incubated at 37°C, spun down to separate the entrapped DiI and the released DiI in the supernatant, and fluorescence was measured on microplate spectrophotometer. **Figure 11** shows that there was no observable reduction in fluorescence in the resuspended pellet. Evidence suggests that DiI is stably maintained within the nanoparticle, and that fluorescence detected during flow cytometry is a result of the detection of fluorescence within the nanoparticle. To understand the localization of the nanoparticles within the cell, **Figure 9 and 10** show that nanoparticles are highly concentrated throughout non-nuclear contents of the cell, presumably in the cytoplasm and in the endocytic pathway.

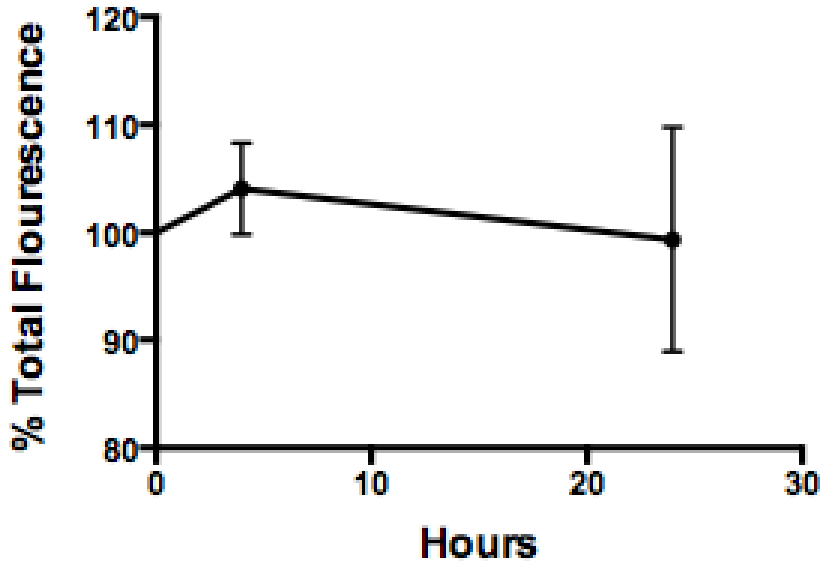

Figure 11. DiI PLGA nanoparticles are stable in cell media-like solution. Nanoparticles were washed and suspended in 1% BSA in PBS, then incubated at 37°C for 0h, 4h, and 24h timepoints.

Flow cytometry was performed to show preferential uptake of nanoparticles by macrophages. RAWs were co-cultured with 3T3s in a 1:1 ratio and treated either with Mg PLGA nanoparticles (NPs) or DiI NPs. Cells were also either treated with or without LPS. One plate of cells was stimulated with LPS and NP treatment for 3h, while the other plate was stimulated for 24h. Mg-containing, DiI-negative NPs were included as a treatment to control for any auto-fluorescence of the nanoparticles. Gates were set along F4/80 and DiI fluorescence intensities so that cell populations and positive/negative nanoparticle fluorescence could be distinguished. $F4/80^{+}$ cells were indicative of RAWs, while $F4/80^{-}$ cells were indicative of 3T3 cell population.

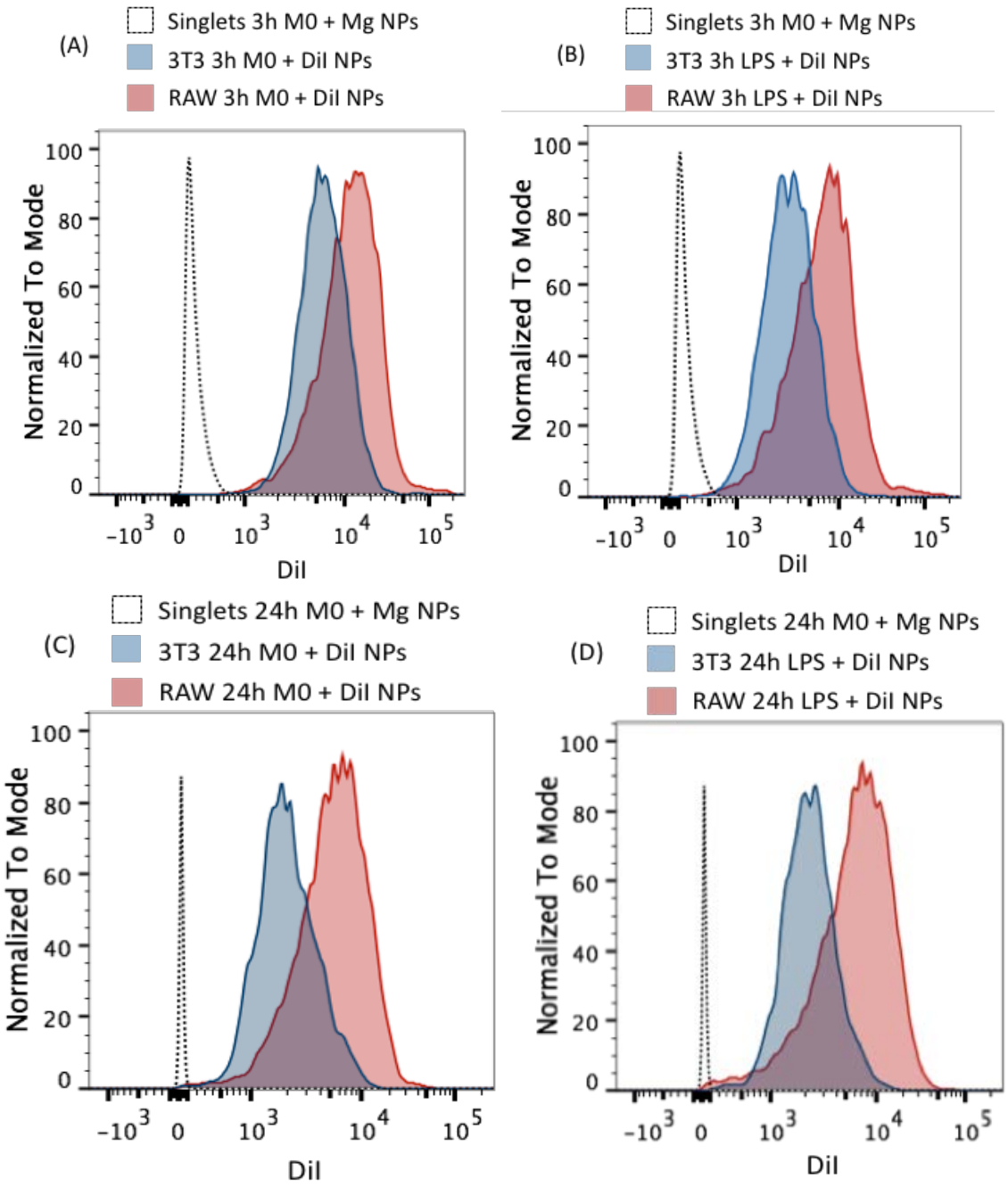

Figure 12. MFI histograms show greater uptake of nanoparticles in RAWs than 3T3s across both timepoints, with differences in uptake greater at 24h (C) (D). RAWs and 3T3s were co-cultured in 6-well plates, stimulated for either 3h or 24h with treatment, and stained with F4/80 APC-Cy7. Flow cytometry was performed with lasers for PE and APC-Cy7 for detection of fluorescence from nanoparticles and F4/80. $F4/80^{+}$ cells were gated to represent the RAW cell population, and $F4/80^{-}$ cells were represented as 3T3s. To gate for PE, cells stained with F4/80 APC-Cy7 but treated with non-fluorescent particles were also analyzed by flow cytometry. Gates were drawn approximately around the PE signal for this group. MFI were obtained from analyzing data via FlowJo.

Treatment	Cell type	MFI	MFI_{RAW}/MFI_{3T3}
3h M0 + Mg NPs	3T3 + RAW	155	--
3h M0 + DiI NPs	3T3	6133	--
3h M0 + DiI NPs	RAW	12438	2.028
3h LPS + DiI NPs	3T3	3246	--
3h LPS + DiI NPs	RAW	7414	2.284

Table 1. MFI is greater in RAWs than 3T3s by at least a factor of 2 in both M0 and M1 cells. MFI difference between RAW and 3T3 is slightly greater among LPS treated cells vs. non-LPS treated cells at 3h.

Treatment	Cell type	MFI	MFI_{RAW}/MFI_{3T3}
24h M0 + Mg NPs	3T3 + RAW	125	--
24h M0 + DiI NPs	3T3	2065	--
24h M0 + DiI NPs	RAW	5731	2.775
24h LPS + DiI NPs	3T3	2000	--
24h LPS + DiI NPs	RAW	7054	3.527

Table 2. MFI is greater in RAWs than 3T3s by at least a factor of 2 in both M0 and M1 cells. MFI difference between RAW and 3T3 is measurably greater among LPS treated cells vs. non-LPS treated cells at 24h.

Median fluorescence intensities (MFI) were plotted from dot plots. **Figure 12** shows higher relative uptake of nanoparticles in RAWs than 3T3s at both time points and with or without LPS. Negligible auto-fluorescence of the nanoparticles was observed. The histograms are plotted on the log scale; RAWs typically had twice the fluorescence intensity of 3T3s. More pronounced differences in MFI between cell types exist at 24h, suggesting that preferential uptake of nanoparticles by macrophages is maintained throughout at least a 24h time period **(Table 2).** Differences in MFI between cell types is also higher in LPS treated groups vs. non-LPS treated groups **(Table 1 and 2)**. Evidence supports that M1 macrophages can be preferentially targeted by our nanoparticles.

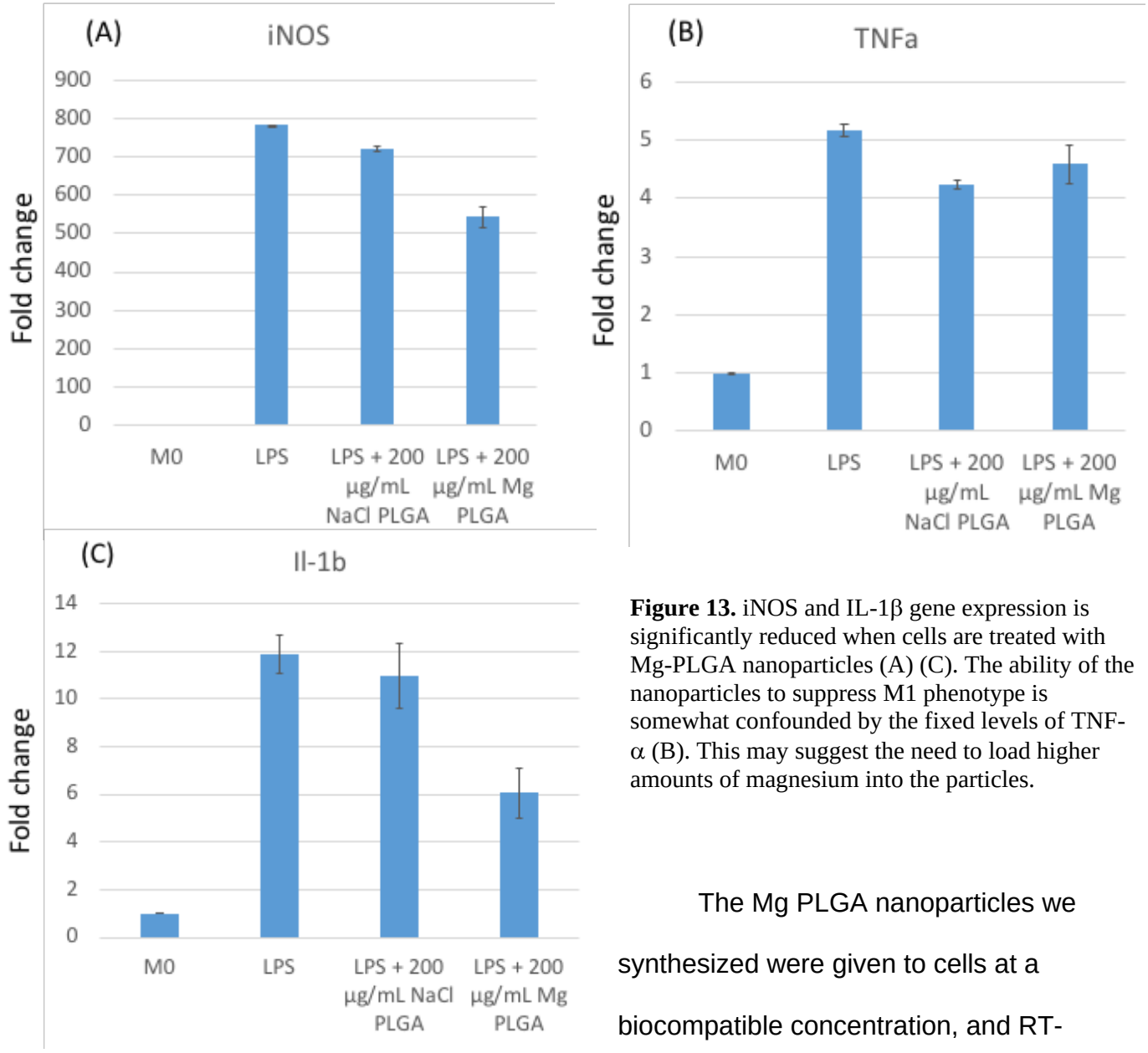

Figure 13. iNOS and IL-1β gene expression is significantly reduced when cells are treated with Mg-PLGA nanoparticles (A) (C). The ability of the nanoparticles to suppress M1 phenotype is somewhat confounded by the fixed levels of TNF-α (B). This may suggest the need to load higher amounts of magnesium into the particles.

The Mg PLGA nanoparticles we synthesized were given to cells at a biocompatible concentration, and RT-PCR was performed. iNOS and IL-1β were significantly reduced in activated macrophages treated with Mg-PLGA compared to activated macrophages without the nanoparticles, but TNF-α levels remained relatively unchanged **(Figure 13B)**. The iNOS knockdown showed that our nanoparticles were capable of reducing the expression of the primary gene that we know to induce muscle lysis during regeneration. IL-1β knockdown further supports the capability of the nanoparticles to reduce M1 gene

expression. However, TNF-α remains as a key player in regulating the inflammatory response, and was not reduced in expression. Loading more magnesium into the nanoparticles should be explored, as TNF-α expression was highly reduced in the RT-PCR data for cells treated with $MgSO_4$ **(Figure 5B)**. By delivering a higher concentration of magnesium to macrophages through the nanoparticles, M1 phenotype may be further reduced. Lactic acid seems to have played less of a role in mediating the changes in gene expression: RAWs treated with nanoparticles loaded with NaCl did not significantly reduce gene expression in any of the three major M1 genes (**Figure 13)**. The concentration of lactate in the cell due to hydrolysis of PLGA may not be high enough to stimulate changes in gene expression, at least in the course of this 24h experiment. The time scales of a 24h experiment does not match the time scale of PLGA degradation, which is on the order of days [29]. Nevertheless, PLGA presents itself as an extremely promising candidate as a carrier for delivering drugs to macrophages.

Conclusion and Future Studies

Macrophage phenotype can be exploited to resolve inflammation in the context of muscle repair to improve tissue regeneration. We were able to successfully synthesize PLGA nanoparticles with entrapped magnesium and deliver them to macrophages to reduce M1 phenotype. This inexpensive, stable nanoparticle formulation reduced the expression of key M1 genes, such as iNOS and IL-1β. Results were telling that magnesium played more of a role in reducing this phenotype than lactic acid, but PLGA was able to act as a stable carrier for drug delivery. PLGA nanoparticles were shown to be preferentially taken up by macrophages, suggesting that the effects of introducing this nanoparticle to other cell types in the body is limited upon injection. Future work involves treating human cell lines with the nanoparticles and translating nanoparticle treatment experiments *in vivo*. Targeting strategies to increase specificity for macrophages should also be studied. *In vivo* experiments would involve inducing skeletal muscle injury in mice, such as ischemia-reperfusion injury, and injecting nanoparticles at the site of injury. Histological analysis of muscle repair would be studied as an output of success.

References

1. Chan O, Buono AD, Best TM, Maffulli N. Acute muscle strain injuries: a proposed new classification system. *Knee Surgery, Sports Traumatology, Arthroscopy*. 2012;20(11):2356-2362. doi:10.1007/s00167-012-2118-z

2. Baoge L, Van Den Steen E, Rimbaut S, et al. Treatment of skeletal muscle injury: a review. *ISRN Orthop*. 2012;2012:689012. Published 2012 Apr 26. doi:10.5402/2012/689012

3. Maffulli N, Del Buono A, Oliva F, et al. Muscle Injuries: A Brief Guide to Classification and Management. *Transl Med UniSa*. 2014;12:14–18. Published 2014 Sep 1.

4. E. D. Arrington and M. D. Miller. Skeletal muscle injuries. *Orthopedic Clinics of North America*. 1995;26(3): 411–422.

5. Toumi H, Best TM. The inflammatory response: friend or enemy for muscle injury? *Br J Sports Med*. 2003;37(4):284–286. doi: 10.1136/bjsm.37.4.284.

6. Laumonier T, Menetrey J. Muscle injuries and strategies for improving their repair. *J Exp Orthop*. 2016;3(1):15. doi:10.1186/s40634-016-0051-7

7. Collins CA. Satellite cell self-renewal. *Curr Opin Pharmacol.* 2006;6(3):301–306. doi: 10.1016/j.coph.2006.01.006.

8. Fernandes TL, Pedrinelli A, Hernandez AJ. Muscle injury - physiopathology, diagnosis, treatment and clinical presentation. *Rev Bras Ortop*. 2015;46(3):247–255. Published 2015 Dec 8. doi:10.1016/S2255-4971(15)30190-7

9. Smith, C., Kruger, M.J., Smith, R.M. The inflammatory response to skeletal muscle injury: illuminating complexities. *Sports Med* (2008);38: 947. https://doi.org/10.2165/00007256-200838110-00005

10. Arnold L, Henry A, Poron F, Baba-Amer Y, van Rooijen N, Plonquet A, Gherardi RK, Chazaud B. Inflammatory monocytes recruited after skeletal muscle injury switch into antiinflammatory macrophages to support myogenesis. *J Exp Med.* 2007;204:1057–1069.

11. Bryer SC, Fantuzzi G, Van Rooijen N, Koh TJ. Urokinase-type plasminogen activator plays essential roles in macrophage chemotaxis and skeletal muscle regeneration. *J Immunol* 2008; 180: 1179 –1188.

12. Lu H, Huang D, Ransohoff RM, Zhou L. Acute skeletal muscle injury: CCL2 expression by both monocytes and injured muscle is required for repair. *FASEB J* 2011;25: 3344 –3355.

13. Mills CD, Kincaid K, Alt JM, Heilman MJ, Hill AM. M-1/M-2 Macrophages and the Th1/Th2 Paradigm. *The Journal of Immunology.* 2000;164(12):6166-6173; doi: 10.4049/jimmunol.164.12.6166

14. Sica A, Mantovani A. Macrophage plasticity and polarization: in vivo veritas. *J Clin Invest*. 2012;122(3):787–795. doi:10.1172/JCI59643

15. Saclier M, Yacoub-Youssef H, Mackey AL, et al. Differentially Activated Macrophages Orchestrate Myogenic Precursor Cell Fate During Human Skeletal Muscle Regeneration. *Stem Cells*. 2013;31(2):384-396. doi:10.1002/stem.1288

16. Rath M, Müller I, Kropf P, Closs EI, Munder M. Metabolism via Arginase or Nitric Oxide Synthase: Two Competing Arginine Pathways in Macrophages. *Front Immunol*. 2014;5:532. Published 2014 Oct 27. doi:10.3389/fimmu.2014.00532

17. Saccani A, et al. p50 nuclear factor-kappaB overexpression in tumor-associated macrophages inhibits M1 inflammatory responses and antitumor resistance. *Cancer Res.* 2006;66(23):11432–11440. doi: 10.1158/0008-5472.CAN-06-1867.

18. Guiducci C, Vicari AP, Sangaletti S, Trinchieri G, Colombo MP. Redirecting in vivo elicited tumor infiltrating macrophages and dendritic cells towards tumor rejection. *Cancer Res.* 2005;65(8):3437–3446.

19. W. D. Hammers et al. “Anti-inflammatory macrophages improve skeletal muscle recovery from ischemia-reperfusion,” *Applied Physiology* 118: 1067-1074, Feb. 2015.

20. B. Deng et al. Interleukin-10 triggers changes in macrophage phenotype that promote muscle growth and regeneration. *The Journal of Immunology* 2013;189: 3669-3680.

21. Nguyen HX, Tidball JG. Interactions between neutrophils and macrophages promote macrophage killing of rat muscle cells in vitro. *J Physiol*. 2002;547:125–132. doi:10.1113/jphysiol.2002.031450

22. O. R. Colegio et al. Functional polarization of tumour-associated macrophages by tumour- derived lactic acid. *Nature.* 2014; 513: 559-563

23. Xianmin Mu, Wei Shi, Yue Xu, Che Xu, Ting Zhao, Biao Geng, Jing Yang, Jinshun Pan, Shi Hu, Chen Zhang, Juan Zhang, Chao Wang, Jiajia Shen, Yin Che, Zheng Liu, Yuanfang Lv, Hao Wen & Qiang You. Tumor-derived lactate induces M2 macrophage

polarization via the activation of the ERK/STAT3 signaling pathway in breast cancer, *Cell Cycle*. 2018;17:4, 428-438, doi: 10.1080/15384101.2018.1444305

24. Sugimoto J, Romani AM, Valentin-Torres AM, et al. Magnesium decreases inflammatory cytokine production: a novel innate immunomodulatory mechanism. *J Immunol*. 2012;188(12):6338–6346. doi:10.4049/jimmunol.1101765

25. Liu T, Zhang L, Joo D, Sun SC. NF-κB signaling in inflammation. *Signal Transduct Target Ther*. 2017;2:17023. doi:10.1038/sigtrans.2017.23

26. Murphy KM. Janeway's Immunobiology, 8th edn. Garland, 2010.

27. Ferrari M. Cancer nanotechnology: opportunities and challenges. *Nat Rev Cancer*. 2005;5(3):161–171.

28. Ruoslahti E, Bhatia SN, Sailor MJ. Targeting of drugs and nanoparticles to tumors*. J Cell Biol.* 2010;188(6):759–768.

29. Gentile P, Chiono V, Carmagnola I, Hatton PV. An overview of poly(lactic-co-glycolic) acid (PLGA)-based biomaterials for bone tissue engineering. *Int J Mol Sci*. 2014;15(3):3640–3659. Published 2014 Feb 28. doi:10.3390/ijms15033640

30. Ding AG, Schwendeman SP. Acidic microclimate pH distribution in PLGA microspheres monitored by confocal laser scanning microscopy. *Pharm Res*. 2008;25(9):2041–2052. doi:10.1007/s11095-008-9594-3

31. Makadia HK, Siegel SJ. Poly Lactic-co-Glycolic Acid (PLGA) as Biodegradable Controlled Drug Delivery Carrier. *Polymers (Basel)*. 2011;3(3):1377–1397. doi:10.3390/polym3031377

32. Huang W, Zhang C. Tuning the Size of Poly(lactic-co-glycolic Acid) (PLGA) Nanoparticles Fabricated by Nanoprecipitation. *Biotechnol J*. 2017;13(1):10.1002/biot.201700203. doi:10.1002/biot.201700203

33. McCall RL, Sirianni RW. PLGA nanoparticles formed by single- or double-emulsion with vitamin E-TPGS. *J Vis Exp*. 2013;(82):51015. Published 2013 Dec 27. doi:10.3791/51015

34. Alan Aderem, Phagocytosis and the Inflammatory Response, *The Journal of Infectious Diseases*. 2003;187(2):S340–S345, https://doi.org/10.1086/374747

35. Parameswaran N, Patial S. Tumor necrosis factor-α signaling in macrophages. *Crit Rev Eukaryot Gene Expr*. 2010;20(2):87–103.

36. Gabay C. Interleukin-6 and chronic inflammation. *Arthritis Res Ther*. 2006;8 Suppl 2(Suppl 2):S3. doi:10.1186/ar1917

37. Fernando MR, Reyes JL, Iannuzzi J, Leung G, McKay DM. The pro-inflammatory cytokine, interleukin-6, enhances the polarization of alternatively activated macrophages. *PLoS One*. 2014;9(4):e94188. Published 2014 Apr 15. doi:10.1371/journal.pone.0094188

38. Guo CJ, Douglas SD, Lai JP, et al. Interleukin-1beta stimulates macrophage inflammatory protein-1alpha and -1beta expression in human neuronal cells (NT2-N). *J Neurochem*. 2003;84(5):997–1005.

39. Jungi, T., Adler, H., Adler, B., Thöny, M., Krampe, M., & Peterhans, E. (1996). Inducible nitric oxide synthase of macrophages. Present knowledge and evidence for species-specific regulation. *Veterinary Immunology and Immunopathology;* 54(1-4), 323-330. doi:10.1016/s0165-2427(96)05690-5

40. Jablonski, K. A., Amici, S. A., Webb, L. M., Ruiz-Rosado, J. D., Popovich, P. G., Partida-Sanchez, S., & Guerau-De-Arellano, M. Novel Markers to Delineate Murine M1 and M2 Macrophages. *Plos One.* 2015;10(12). doi:10.1371/journal.pone.0145342

41. Williams, L., Bradley, L., Smith, A., & Foxwell, B. Signal Transducer and Activator of Transcription 3 Is the Dominant Mediator of the Anti-Inflammatory Effects of IL-10 in Human Macrophages. *The Journal of Immunology.* 2003;*172*(1), 567-576. doi:10.4049/jimmunol.172.1.567

42. Gerard, C., C. Bruyns, A. Marchant, D. Abramowicz, P. Vandenabeele, A. Delvaux, W. Fiers, M. Goldman, and T. Velu. Interleukin 10 reduces the release of tumor necrosis factor and prevents lethality in experimental endotoxemia. *J. Exp. Med.* 1993;177:547.

43. Martinez FO, Gordon S. The M1 and M2 paradigm of macrophage activation: time for reassessment. *F1000Prime Rep*. 2014;6:13. Published 2014 Mar 3. doi:10.12703/P6-13

44. Schmittgen, T. D., & Livak, K. J. (2008). Analyzing real-time PCR data by the comparative CT method. *Nature Protocols,3*(6), 1101-1108. doi:10.1038/nprot.2008.73

45. Bryan NS, Grisham MB. Methods to detect nitric oxide and its metabolites in biological samples. *Free Radic Biol Med*. 2007;43(5):645–657. doi:10.1016/j.freeradbiomed.2007.04.026

46. Riss TL, Moravec RA, Niles AL, et al. Cell Viability Assays. 2013.

47. Champion JA, Walker A, Mitragotri S. Role of particle size in phagocytosis of polymeric microspheres. *Pharm Res*. 2008;25(8):1815–1821. doi:10.1007/s11095-008-9562-y